HHS Public Access

Author manuscript

Cell. Author manuscript; available in PMC 2017 January 14.

Published in final edited form as:

Cell. 2016 January 14; 164(1-2): 156–169. doi:10.1016/j.cell.2015.11.058.

WNT-SHH Antagonism Specifies and Expands Stem Cells Prior to Niche Formation

Tamara Ouspenskaia[1], **Irina Matos**[1], **Aaron F. Mertz**[1], **Vincent F. Fiore**[1], and **Elaine Fuchs**[1,*]

Tamara Ouspenskaia: touspenska@rockefeller.edu; Irina Matos: imatos02@rockefeller.edu; Aaron F. Mertz: aaron.mertz@rockefeller.edu; Vincent F. Fiore: vfiore@rockefeller.edu; Elaine Fuchs: fuchslb@rockefeller.edu

[1]Robin Neustein Laboratory of Mammalian Development and Cell Biology, Howard Hughes Medical Institute, The Rockefeller University, New York NY 10065

Abstract

Adult stem cell (SC) maintenance and differentiation are known to depend on signals received from the niche. Here however, we demonstrate a mechanism for SC specification and regulation that is niche-independent. Using immunofluorescence, live imaging, genetics, cell-cycle analyses, *in utero* lentiviral transduction, and lineage-tracing, we show that in developing hair buds, SCs are born from asymmetric divisions that differentially display WNT and SHH signaling. Displaced WNT^{lo} suprabasal daughters become SCs that respond to paracrine SHH and symmetrically expand. By contrast, basal daughters remain WNT^{hi}. They express but do not respond to SHH, and hence maintain slow-cycling, asymmetric divisions. Over time, they become short-lived progenitors, generating differentiating daughters rather than SCs. Thus, in contrast to an established niche which harbors a fixed SC pool whose expelled progeny differentiate, asymmetric divisions first specify and displace early SCs into an environment conducive to expansion, and later restrict their numbers by switching asymmetric fates.

INTRODUCTION

Adult tissues are maintained and repaired by resident stem cells (SCs), which are capable of long-lived self-renewal and differentiation into one or more cell types. SC behavior depends on signals received from neighboring differentiated cells—referred to as the “niche” (Scadden, 2014; Schofield, 1978). As recent studies have shown, SC niche components can include SC progeny as well as heterologous cell types (Hsu et al., 2014; Hsu et al., 2011), and SCs can also signal to their early progeny (Pardo-Saganta et al., 2015). In this niche-centric view, the microenvironment provides the requisite signals, such that, upon exit from the niche, “stemness signals” are no longer received in sufficient doses, and the cells acquire

*To whom correspondence should be addressed: Elaine Fuchs, Rebecca Lancefield Professor, Howard Hughes Medical Institute, The Rockefeller University, 1230 York Avenue, Box 300, New York, NY 10065, fuchslb@rockefeller.edu; TEL: 212-327-7953; FAX: 212-327-7954.

SUPPLEMENTAL INFORMATION

Supplemental Information includes Supplemental Experimental Procedures, 5 figures, and 5 movies.

a different fate. In this manner, the number of SCs is predicated on both the signals and the numbers of available positions within a pre-existing niche.

The overarching importance of the niche in maintaining SC identity and number inspires the question of how SCs are specified during development. In the majority of described models, SC establishment relies on signals emanating from a pre-established niche. In *Drosophila* gonads, the SC niche acts as a signaling center to recruit and maintain germ SCs from among a small population of undifferentiated primordial germ cells (PGCs) (Dansereau and Lasko, 2008). PGCs outside of the niche directly enter cyst (females) or gonialblast (males) differentiation pathways (Bhat and Schedl, 1997; Song et al., 2002; Zhu and Xie, 2003). In the developing intestine, cells expressing SC marker LGR5 are initially present throughout the epithelium. They become confined to the crypt base as the villus buckles, thereby concentrating differentiation signals within the upper tip region (Shyer et al., 2015). These examples demonstrate how existence of a niche can determine the location and number of SCs. An intriguing question still unaddressed is whether SCs are formed prior to niche establishment. If so, there must be some alternative way in which their identity and numbers are controlled.

The hair follicle (HF) is an excellent system in which to explore these questions. Skin begins as one layer of unspecified epidermal progenitors. In mice, from embryonic day E14.5 to birth, hair placodes emerge in waves of spatially patterned cell clusters within the basal–epidermal plane. Canonical WNT-signaling, mediated by β-catenin and LEF1, is essential for placode formation (Andl et al., 2002; Gat et al., 1998; Huelsken et al., 2001; van Genderen et al., 1994). The initial step appears to take place in the absence of cell divisions, as WNT-signaling epidermal cells cluster within the basal plane (Ahtiainen et al., 2014). Other than established links to both WNT- and SHH-signaling, it is unclear how molecular and cellular diversity are then generated as the placode grows downward to form a bud (hair germ). While both signals occur within the bud, SHH-signaling is genetically downstream of WNT-signaling, as it still occurs when SHH is absent, even though hair buds but do not progress further (Jamora et al., 2003; St-Jacques et al., 1998; Woo et al., 2012).

Lineage tracing has established that a pool of slow-cycling cells with molecular characteristics of adult HFSCs exists as early as E18.5, at a stage when developing HFs are nearing maturity and their “bulge” niche within the outer root sheath (ORS) has formed (Nowak et al., 2008). At first glance, this result would seem to support the pre-formed niche hypothesis for SC establishment. However, recent epigenetic studies suggest that, although the niche microenvironment dictates many molecular features of SCs, SCs can survive outside their niche if they can adapt their chromatin landscape to a new microenvironment (Adam et al., 2015). In this regard, only a few markers of SCs in their native niche may actually be essential for SC identity.

For adult HFSCs, the key to retaining stemness outside the bulge is SOX9 (Adam et al., 2015). Intermediate levels of SOX9 characteristic of wound-repair and cell culture are insufficient to sustain the cohort of other genes expressed by HFSCs in their niche. However, these levels are enough to endow SCs with plasticity and enable them to adopt either epidermal or HF fates. Since SOX9 is first expressed during epithelial budding in the

absence of the full regalia of bulge HFSC markers, we speculated that HFSC specification might occur at this early stage. If so, specification would occur long before niche establishment.

In this study, we examine how molecular and cellular diversity is generated within the hair germ, and explore roles that WNTs and SHH play in SC specification and in balancing proliferation and differentiation at a time before the niche has been established. Unexpectedly, we find that the earliest divisions within the established WNT^{hi} placode are exclusively perpendicular to the underlying basement membrane. Using genetic mosaic approaches, we provide compelling evidence that the purpose of these perpendicular divisions within the native placode is to place one daughter outside of its WNT^{hi} parent cell environment. Using live imaging, whole-mount immunofluorescence microscopy, and short-term lineage tracing, we further show that these divisions achieve asymmetrically partitioned WNT- and SHH-signaling, establishing a discrete molecular platform for two cell fates to emerge.

Hitherto unappreciated, the displaced WNT^{lo} suprabasal daughter becomes a SC progenitor that expresses SOX9. Moreover, although the WNT^{hi} basal parent is the source of SHH, only its WNT^{lo} suprabasal daughter can respond. Intriguingly, the $SOX9^{+}$ SC daughter undergoes rapid symmetric divisions, which appear to be SHH-dependent, while the basal parent continues to divide slowly and asymmetrically, a process which appears to be associated with its WNT^{hi} state. This progression differs markedly from a pre-established niche, in which hub vacancies govern whether SCs will proliferate. Importantly, and again in contrast to a pre-established niche, in which niche site occupancy dictates the maximum number of SCs, here, early HFs use different means to halt SC production. As WNT^{hi} parents mature into short-lived progeny, their slow-cycling asymmetric divisions shift, and, instead of spawning SC daughters, they start to generate differentiating daughters. Overall, our findings show that SCs can be born by displacement from their parental environment during morphogenesis, and reveal how asymmetric distribution of WNT and SHH signaling and their mutual antagonism are used in the niche's place to govern SC specification and balance proliferation and differentiation.

RESULTS

Each Division in Hair Placodes Generates a Basal and a Suprabasal Daughter

To understand how cell fates are specified in early HF morphogenesis, we investigated the first cell divisions that occur following placode formation. Immunolabeling for acetylated tubulin decorated the stable spindle microtubules and the cleavage furrow of mitotic cells, and P-cadherin (Pcad) distinguished placodes from interfollicular epidermis (IFE).

Unexpectedly, nearly all mitotic spindles within ($Pcad^{hi}$) hair placodes were oriented perpendicular (>45° angle) to the underlying basement membrane (Figure 1A). Quantitative analysis of an additional cleavage furrow marker, survivin, was suggestive of a perpendicular bias of late-stage mitotic division planes within these early stages of epithelial budding (Figure 1B). Hitherto overlooked, the nearly exclusive perpendicular angling further distinguished hair placodes from IFE, where such perpendicular spindles are fewer and have

been linked to early steps involved in forming the skin barrier (Clayton et al., 2007; Lechler and Fuchs, 2005; Williams et al., 2014).

To ascertain whether perpendicular spindle orientations resolve into basal and suprabasal daughters, we developed a method to perform 4D video-microscopy on immobilized, *ex utero* E14.5 mouse embryos whose epidermis expressed a fluorescently tagged histone gene (*Krt14*–H2BGFP). Placodes were readily identified by their tight cell packing and hexagonal organization (Figure 1C). In total, we measured relative positions of daughters from 322 basal placode divisions (Movie S1).

Parallel divisions were largely confined to IFE (Figure 1D; Movie S2). By contrast, divisions within placodes were nearly exclusively vertical, leaving one daughter at −3μm and one daughter at +6μm relative to the basal plane (Figure 1E; Movie S3). Together, these data showed that perpendicular spindle orientations within the skin result in a basal daughter that remains attached to the basement membrane and a suprabasal daughter that is born unattached (Figure 1E, schematic). Our movies corroborated our spindle axis measurements and showed an equal proportion of parallel and perpendicular divisions in basal IFE, but almost exclusively perpendicular divisions in basal placodes (Figure 1F).

Perpendicular Divisions in Developing Hair Placodes Asymmetrically Partition WNT-signaling and Generate Suprabasal Progeny with Features of Early Stem Cells

Whole-mount immunofluorescence of late-stage mitoses within placodes revealed that basal daughters differentially inherited Pcad, indicating that these perpendicular divisions are asymmetric (Figure 2A,B). LGN binds to Gαi, links mitotic spindles to the apical PAR3/aPKC complex, and promotes asymmetric divisions in IFE (Williams et al., 2011; Williams et al., 2014). Interestingly, LGN was also localized apically in perpendicular, late-stage mitotic placode cells, resulting in its asymmetric distribution to suprabasal daughters (Figure 2C).

Since WNT-signaling is high in placodes and required for their formation, we monitored its fate when placode cells begin to divide. Surprisingly, only basal daughters exhibited intense nuclear LEF1, suggestive of active, short-range WNT-signaling. Strong basal activity of WNT-reporter Axin2-LacZ (Lustig et al., 2002) confirmed that WNT-signaling was high/retained by daughters that remained attached to underlying basement membrane (Figure 2D). Furthermore, activated focal adhesion kinase (FAK) and β1-integrin concentrated on the basement membrane-associated side of WNT^{hi} basal placode cells (Figure 2E). The ability of activated FAK to phosphorylate and inactivate GSK3β (Gao et al., 2015) should further favor β-catenin stabilization basally and restrict GSK3β-mediated phosphorylation and proteosomal degradation to the apical domain.

While placode transcription factors LHX2 and LEF1 were nuclear and basal (Figure 2F, left) (Rhee et al., 2006), suprabasal daughter nuclei were often positive for the SC pioneer factor SOX9 (Figures 2F, right; S1, planar view). These findings suggested that LHX2/LEF1/$AxinLacZ^{+}$ basal placode cells may divide asymmetrically to generate suprabasal daughters that become $SOX9^{+}$. To test that possibility, we used *in utero* transduction to selectively infect the single layer of surface ectoderm of E9.5 embryos with lentivirus (LV), which by

24–48h, stably integrates into the host genome and is thereafter propagated to progeny (Beronja et al., 2010). We infected *Rosa26-fl-STOP-fl-YFP* (*R26YFP*$^{fl/+}$) embryos with LV expressing an inducible CreER recombinase (LV-Cre) (Figure 2G). Low-dose tamoxifen at E15.5 activated CreER in isolated cells throughout the skin. Shortly thereafter, several small YFP^{+} clones with Pcad^{hi} basal and SOX9^{+} suprabasal cells were detected within hair placodes (Figure 2H). These data were consistent with the notion that outcomes of these early asymmetric cell divisions were asymmetric fates. We revisit this idea in more detail later.

Differential WNT-signaling is Key for Coupling Asymmetric Fates to Asymmetric Cell Divisions

Based upon loss-of-function studies with β-catenin and gain-of-function studies with the direct WNT inhibitor DKK1 (Andl et al., 2002; Huelsken et al., 2001) (Figure S2), WNT-signaling is essential to make placodes. If the purpose of the subsequent perpendicular divisions within placodes is to release suprabasal daughters from the high-WNT-signaling environment of their parents, then super-activation of WNT-signaling should prevent SOX9+ cell specification. We tested this possibility by mosaically ablating the gene encoding APC, a member of the AXIN-APC-GSK3β complex that sequesters and targets non-junctional β-catenin for phosphorylation and proteosome-mediated degradation (Azzolin et al., 2014; Li et al., 2012; Mendoza-Topaz et al., 2011).

Given the severity of conditionally ablating *Apc* in skin (Kuraguchi et al., 2006), we infected E9.5 *Apc*$^{fl/fl}$*; R26YFP*$^{fl/+}$ embryos with low-titer LV-Cre. Small mosaic patches of *Apc*-null-derived YFP^{+} epidermal cells exhibited robust WNT-signaling as evidenced by elevated nuclear β-catenin and LEF1 (Figure 3A,B). Notably, the *Apc*-null patches were LHX2^{+} and devoid of SOX9, indicating a skewing of fates relative to their wild-type counterparts.

Within the basal plane, a halo of WT SOX9^{+} cells surrounded the *Apc*-null patches (Figure 3B). Since the SOX9^{+} halo was *Apc*^{WT} while LHX2^{+} cells were *Apc*-null, halo cells could not have been generated by asymmetric cell divisions. Rather, the unifying feature between this mosaic, genetically altered skin and native, asymmetrically dividing skin placodes was differential levels of WNT-signaling in LHX2^{+} versus SOX9^{+} neighbors.

To pursue the hypothesis that specification of SOX9^{+} cells is dependent on juxtaposing WNT^{lo} cells with WNT^{hi} ones, we tested the reverse, namely the consequences to asymmetric cell fates when mosaic clones null for the β-catenin gene (*Ctnnb1*) were juxtaposed with WT clones. In WT patches, nuclear LEF1 was seen throughout IFE, even though it was higher in hair placodes. By contrast, *Ctnnb1*-null epidermal patches lacked not only β-catenin, but also nuclear LEF1 (Figure 3C). Basal placode markers LHX2 and high Pcad were also not found in *Ctnnb1*-null patches, further underscoring the requirement of WNT-signaling for placode formation (Figure 3D). Notably, however, a halo of SOX9-expressing *Ctnnb1*-null epidermal cells surrounded WT placodes. As demonstrated by LV-Cre-mediated YFP^{+} lineage tracing, these SOX9^{+} cells remained in the epidermis and did not migrate into or contribute to HFs (Figure 3E).

Together, these gain- and loss-of-function studies provided compelling evidence that the key feature enabling SOX9^{+} cell specification is juxtaposition of WNT^{hi} and WNT^{lo} signaling cells. In developing HFs, this juxtaposition appeared to be achieved through asymmetric cell divisions, displacing the suprabasal daughter from the WNT^{hi} environment of its parent and linking asymmetric fates to asymmetric divisions. Our findings show that if this condition is met by other means (e.g., through mosaic genetic mutation), asymmetric divisions are not needed to generate asymmetric fates.

WNT^{hi} Daughters Divide Infrequently

In many cell types, WNT-signaling is thought to promote self-renewal and proliferation (Clevers et al., 2014; Pei et al., 2012; Reya et al., 2003; Shin et al., 2011). Since both WNT^{hi} and WNT^{lo} cells emerged within the epithelial bud, we sought to know the proliferative status of these two populations. To address this issue, we mated *Axin2-LacZ* mice onto the *Fucci* background, which labels nuclei of G_1/G_0 cells with monomeric Kusabira-Orange 2 (mKO2) (Ahtiainen et al., 2014; Sakaue-Sawano et al., 2008).

As expected, short-term labeling with nucleotide analogue 5′-ethynyl-2′-deoxyuridine (EdU) showed little or no overlap with mKO2^{+} cells. In the epidermis, mKO2 marked nuclei in terminally differentiating suprabasal layers (Figure 4A, asterisks). Within hair germs, however, mKO2 marked WNT^{hi} LHX2^{+} basal cells. Quantitative flow cytometry analysis confirmed that, in total, ~20% of hair germ cells were mKO2^{hi} (Figures 4B; S3A). This result was in stark contrast to IFE, where only 2% of α6^{hi} cells were mKO2^{hi}.

The mKO2^{hi} population was accentuated when β-catenin stabilization was enhanced genetically (Figures 4C,D; S3B), thereby reinforcing the notion that, in developing epithelial buds *in vivo*, high WNT-signaling slows proliferation. That said, the WNT^{hi} cells appeared to be in an extended G_1 rather than a G_0 state, since asymmetric divisions within this basal pocket were still seen at the hair germ and peg stages, and since occasional EdU^{+} cells were captured within this pocket (Figure 4E). From these data, we concluded that the early WNT^{hi} basal cells within the HF not only divide asymmetrically, but do so infrequently. These coupled behaviors ensure that the pocket of WNT^{hi} cells, established during placode formation, maintains a constant position and small size throughout HF morphogenesis. Such features also provide little opportunity for these basal cells to alter WNT signaling through cell divisions and/or changes in microenvironment.

SOX9^{+} Cells That are Generated by Asymmetric Divisions Expand Symmetrically

In contrast to WNT^{hi} basal cells, SOX9^{+} WNT^{lo} suprabasal cells showed signs of rapid proliferation and expansion. The first hint of this proliferation came from our live imaging, where we observed divisions within the suprabasal plane of the placode (Figure 5A; Movie S4). In contrast to those of the basal layer, suprabasal divisions within early placodes were exclusively parallel relative to the embryo surface.

Further evidence came from proliferation analysis of SOX9^{+} and LEF1^{+} cells following a short EdU pulse. At the placode stage, SOX9^{+} and LEF1^{+} cells were comparably proliferative, consistent with their derivation from asymmetric divisions (Figure 5B). However, none of the SOX9^{+} cells were mKO2^{hi}, thereby distinguishing suprabasal placode

cells from mKO2^{hi} terminally differentiating epidermal cells and basal WNT^{hi} cells (Figure S4A). Moreover by the hair germ and peg stage, proliferation within the SOX9^{+} population clearly surpassed that in WNT^{hi} LEF1^{+} cells (Figures 5B; S4B).

The positive correlation between proliferation and SOX9 was as striking as the inverse correlation between proliferation and LEF1/WNT-signaling. This correlation was accentuated in the proliferative SOX9^{+} WT IFE halos around WNT^{hi} *Apc*-null non-proliferative patches within *Apc* mosaic skin (Figure 5C).

The consequence of these WNT-dependent differences became increasingly apparent as HF morphogenesis progressed (Figure 5D). While LEF1^{+} WNT^{hi} cell numbers remained constant, SOX9^{+} WNT^{lo} cells expanded. SOX9^{+} cell divisions appeared to be symmetric, with randomized spindle orientations (Figure 5E).

SHH Produced by WNT^{hi} Placode Cells Instigates Symmetric Divisions Only in SOX9^{+} Cells

Our results thus far suggested that SOX9^{+} cell specification is dependent on establishing a WNT-signaling gradient, where WNT^{hi} cells are juxtaposed with WNT^{lo} cells that become SOX9^{+}. Indirectly, however, SOX9^{+} cells still rely on WNT-signaling, since they do not form in complete absence of β-catenin/WNT-signaling and since the *Ctnnb1*-null SOX9^{+} epidermal halos in mosaic skin were restricted to regions juxtaposed to (WNT-responding) WT placodes. One possible explanation is that adjacent WNT^{hi} cells generate a downstream effector, which reinforces SOX9^{+} cell specification and/or expansion. A good candidate was SHH.

We first verified that the basal WNT^{hi} placode cells are positive for *Shh* (Figure S5). As SHH is known to signal to the underlying dermal condensate (Woo et al., 2012), Gli1LacZ reporter activity in these dermal cells was anticipated (Figure 6A). Within developing placodes and germs however, SOX9^{+} cells displayed stronger SHH-reporter activity than basal LEF1/WNT^{hi} cells. Comparing *Shh* expression and WNT and SHH reporter activities, three patterns emerged: 1) Basal hair bud cells produce *Shh* but show only high WNT-signaling and no SHH-signaling; 2) Suprabasal placode cells show low WNT-signaling but elevated SHH-signaling; and 3) Nascent dermal papilla cells exhibit both WNT- and SHH-signaling.

Based on these observations, we posited that, in developing hair buds, high WNT-signaling antagonizes autocrine SHH-signaling. To test this hypothesis, we engineered a mouse model that allowed us to activate *Shh* at different stages in epidermis development. We transduced E9.5 *K14rtTA; Gli1LacZ* embryos with LV harboring a doxycycline-inducible *Shh* cDNA and a PGK-H2BGFP transduction marker (Figure 6B).

When *Shh* was induced at E13.5 and analyzed at E15.5, ectopic paracrine SHH-signaling occurred in the WT IFE cells surrounding GFP^{+} transduced *Shh*-expressing IFE cells (Figure 6C, left). Intriguingly, however, clear signs of autocrine SHH-signaling were also noted, as evidenced by dual presence of H2B–GFP and β-galactosidase. Moreover, regions of ectopic *Shh* showed strong repression of nuclear LEF1, normally present throughout the epidermis (Figure 6C, right). Taken together, these findings suggest that, under conditions

where WNT-signaling is normally present but not robust, SHH activation can override the WNT antagonism and signal in autocrine fashion. Additionally, the data show that, in doing so, SHH-signaling results in repression of WNT-signaling.

To explore this antagonism further, we induced *Shh* at E15.5, i.e., at a stage after HF morphogenesis was initiated. Analyses at E17.5 showed that LEF1 expression in the established WNT^{hi} pocket cells of the HF was refractory to elevated *Shh*, and no signs of fate conversion were observed (Figure 6D).

Finally, if autocrine SHH-signaling is repressed by elevated WNT-signaling, then exclusive paracrine signaling should be observed when WNT-signaling is ectopically elevated. To test this hypothesis, we returned to our mosaic *Apc* model, this time performing qRT-PCR on purified populations of WT and *Apc*-null skin epithelial cells. *Apc*-null cells expressed very high levels of WNT-target gene *Axin2* (Figure 6E). However, while these cells expressed *Shh*, they showed no signs of responding to it, as judged by failure to upregulate SHH target genes *Gli1* and *Ptch1*. Together, these results are consistent with the view that, in cells that do not experience high levels of WNT, paracrine SHH-signaling can occur and suppress WNT-signaling. However, in cells expressing *Shh*, high WNT-signaling prevents autocrine signaling.

To understand the role of SHH-signaling in asymmetric fate specification, we analyzed $SOX9^{+}$ and $LEF1^{+}$ populations in *Shh*-null hair buds. Both daughter types were specified within *Shh*-null placodes (Figure 6F). However, and in striking contrast to WT HFs, $LEF1/WNT^{hi}$ cells were more abundant than $SOX9^{+}$ cells by the hair germ stage (Figure 6G). Moreover, the overall intensity of SOX9 immunofluorescence was reduced in the absence of SHH. Together, these findings suggested that paracrine SHH-signaling is essential not only to expand SOX9-specified cells but also to boost their fate, most likely by suppressing WNT-signaling.

SHH-signaling plays a key role in the recruitment and assembly of the dermal condensate (Karlsson et al., 1999; St-Jacques et al., 1998). However, WNT-signaling perturbations within *Shh*-null hair buds appeared to emanate from epithelial alterations in SHH-signaling, since they still occurred when we selectively ablated *Smoothened* in embryonic skin epithelium. Thus, in the absence of this key receptor for SHH-signaling, the population of WNT^{hi} $LEF1^{+}$ basal cells was expanded, analogous to what we saw in *Shh*-null hair germs (Figure 6H).

Imbalance of $SOX9^{+}$ and $LEF1^{+}$ daughter cells in *Shh*-null hair buds was not caused by defect in spindle positioning during cell divisions, as basal spindle orientations were still exclusively perpendicular to the underlying basement membrane (Figure 6I). These data further underscore the importance of WNT, but not SHH, for these divisions.

Progeny of Early But Not Late Asymmetric Divisions Contribute to the Adult HF Stem Cell Niche

To assess whether early asymmetric cell divisions within the hair bud contribute to the adult HF niche, we used *ShhCreER* lineage tracing (*Sox9CreER* control) to label cells in early

hair buds and trace their fate (Figure 7A). To support our finding that SHH$^+$ cells divide perpendicularly and give rise to suprabasal SOX9$^+$ cells, we labeled SHH$^+$ cells within early hair buds using *ShhCreER; R26mTmG*$^{fl/+}$ embryos. 30h after tamoxifen induction, we performed two-color live imaging of hair placodes, which were the only structures with GFP$^+$ cells (Figure 7B, left). Over 18h of imaging, only a few GFP$^+$ (SHH$^+$) mitoses were observed, consistent with our *Fucci* data showing that SHH$^+$ cells are slow-cycling. However, these divisions were perpendicular, generating one daughter cell atop the other (Figure 7B, right; Movie S5).

Next, we labeled a small number of cells within E14.5→E17.5 *ShhCreER; R26YFP*$^{fl/+}$ hair buds and traced their fates into adulthood. YFP$^+$ cells were seen within the expected domains of emerging placodes and germs (Figure 7C). As predicted from our findings, *Shh*-expressing cells gave rise to SOX9$^+$ daughters, but *Sox9*-expressing cells at these early stages generated only SOX9$^+$ daughters and did not contribute to the WNT^{hi} *Shh*$^+$ pocket. Moreover, progeny from these early *ShhCreER*-marked cells wound up in the adult bulge of SOX9$^+$ SCs, where they were functional and contributed to all SC lineages in subsequent rounds of hair cycling (Figure 7D). Together, these findings support the notion that HFSCs are born from early asymmetric cell divisions.

When lineage tracing was monitored temporally, spatial organization was still consistent with asymmetric cell divisions, but *Shh-CreER* marked progeny now consisted of inner SOX9$^-$ HF layers expressing differentiation markers for the companion layer (Cp; keratin 6) and inner root sheath (IRS; GATA3) (Figure 7E). Taken together, our results fit a model whereby early asymmetric cell divisions by transient *Shh*-expressing parents give rise to SOX9$^+$ SCs, while their later asymmetric cell divisions generate the differentiated cells of the hair lineages.

DISCUSSION

Perpendicular Spindle Orientation and Asymmetric Partitioning of WNT-Signaling Generates Stem Cell Daughters

Before we began our investigation, analyses of spindle orientations in skin were confined to either epidermis (Clayton et al., 2007; Lechler and Fuchs, 2005; Williams et al., 2011) or basal cell carcinomas (BCCs) (Larsimont et al., 2015). It is striking that, in contrast to epidermis where perpendicular spindles peak at ~50–60%, or to BCC where epidermal orientations are randomized, virtually all hair placode spindles are oriented perpendicularly. Our live imaging revealed that perpendicular divisions within the placode generate basal and suprabasal daughters. Our lineage tracing and analyses of molecular markers in late-mitotic doublets established that the outcome of these divisions are asymmetric fates and imply that it is through asymmetric cell divisions that SOX9$^+$ cells are born within the placode.

The relation between placode formation, asymmetric cell division, and SC specification became particularly intriguing when we first observed signs of asymmetric partitioning of WNT-signaling between placode daughters, and subsequently established its functionality and physiological relevance. Growing evidence has suggested that WNTs may be a critical link between SC niche signaling and oriented cell divisions. In the early *C. elegans* embryo,

WNT-signaling is coupled to spindle orientation through polarization of the β-catenin destruction complex (Cabello et al., 2010; Sugioka et al., 2011). In cultured human pluripotent SCs, a polarized bioactive WNT bead applied to one side of the cell surface results in an asymmetric division, with nuclear β-catenin confined to the daughter touching the WNT bead (Habib et al., 2013). In another study, membrane receptors for non-canonical WNT-signaling antagonize canonical WNT-signaling in adult hematopoietic SCs to differentially control proliferative states of daughters (Sugimura et al., 2012). Our findings now suggest a tantalizing possibility that during epithelial bud formation, the basement membrane polarizes and restricts canonical WNT-signaling, such that the pathway becomes asymmetrically partitioned in a perpendicular division.

A myriad of factors could participate in polarizing WNT-signaling to the basal side of placode cells. Heparin sulfate proteoglycans, which can bind and modulate WNT ligands, are enriched within basement membranes (Astudillo and Larrain, 2014; Baeg et al., 2001). The basement membrane is known to polarize a number of surface receptors including integrins that are essential for proper spindle orientation (Lechler and Fuchs, 2005), and similar intertwined or independent interactions could also polarize WNT receptors. Preferential activation of integrins and associated FAK on the basal side of placode cells favors FAK's direct inactivation of GSK3β (Gao et al., 2015) and β-catenin stabilization basally. Conversely, since APC orients mitotic spindles of *Drosophila* germ cells relative to the Hub (Yamashita et al., 2003) and can associate with PAR3/aPKC in mammalian cells (Etienne-Manneville and Hall, 2003; Kodama et al., 2003), the β-catenin destruction complex is favored to be apically enriched. While sifting through these potential mechanisms must await future investigations, the highly polarized placode cells and underlying basement membrane provide an environment conducive to preferentially retaining WNT-signaling in the basal daughter and reducing it in the suprabasal daughter of asymmetric cell divisions.

Uncoupling Asymmetric Fate Specification From Asymmetric Cell Divisions

Suprabasal fates of asymmetrically dividing epidermal and placode cells differ markedly. Based on our findings, these differences appear to be rooted in relative levels of β-catenin/LEF activity within basal progenitors. Indeed, our mosaic loss- and gain-of-function studies provided powerful genetic evidence that WNT-signaling and its associated SHH expression within basal progenitors are critical for reducing WNT-signaling and elevating SHH-signaling in suprabasal placode daughters to a level compatible for SOX9 induction. Importantly, our ability to genetically uncouple asymmetric cell fates from both perpendicular and asymmetric cell divisions by juxtaposing WNT^{hi} and $WNT^{neg/lo}$ cells underscores the importance of asymmetric cell divisions in establishing this condition within the native epithelial bud. This uncoupling also illustrates how changes in microenvironment and/or genetic mutations can alter this dependency. Given the links between WNT signaling, SC biology, and cancer, this understanding is likely to have broad significance for other tissues, both normal and malignant.

Antagonism Between Intrinsic SHH and WNT Signaling in Orchestrating Differential Expansion Between Two Daughter Populations During Morphogenesis

Previously, it was observed that, in E18.5 skin of *Shh*-null or *Gli2*-null embryos, SOX9 is low or absent, and when SMOOTHENED or SHH are superactivated in adult epidermis, SOX9-expressing BCCs develop (Larsimont et al., 2015; Vidal et al., 2005). Our findings not only corroborate these results but also provide further molecular explanation for the observations. Another long-standing mystery is why the *Shh*-expressing pocket in HFs is so small (DasGupta and Fuchs, 1999; Noramly et al., 1999; St-Jacques et al., 1998). Our genetic studies show that elevating WNT-signaling in the hair placode generates SHH, but raises the threshold for autocrine SHH-signaling. Conversely, if WNT-signaling is sufficiently low, the block in autocrine SHH-signaling can be lifted.

Irrespective of mechanism, the outcome of this balanced antagonism between WNT and SHH signaling is that WNT^{hi} basal cells cycle slowly and divide asymmetrically to generate WNT^{lo} daughters, which later become SCs. As our genetic analyses confirm, these features are WNT-dependent and SHH-independent. By contrast, in a SHH-dependent and WNT-independent fashion, SHH-signaling reinforces expression of the SOX9 master regulator and launches rapid symmetrical divisions to expand the SC pool. Genetic perturbation of either WNT-signaling or SHH-signaling specifically within the epithelium is sufficient to skew differential fate outcomes and behaviors.

Solving the Conundrum of Controlling Stem Cell Identity and Numbers in the Absence of a Pre-Established Niche

In adult tissues, the niche defines SC identity and numbers. While niche signaling typically emanates from heterologous cell types, niche SCs can signal to their progeny (Pardo-Saganta et al., 2015) and SC progeny can signal back to their parents (Hsu et al., 2014; Hsu et al., 2011). In all of these cases, however, niche vacancies are sensed and replenished to maintain a fixed SC number. Non-homeostatic vacancies can even be replenished by non-stem cells, further underscoring the importance of the niche microenvironment in dictating SC behavior (Blanpain and Fuchs, 2014).

By studying HF morphogenesis in the embryo, we have now unearthed a very different picture of how SC identity is acquired and how SC numbers are controlled in early development. Here, we discovered that SCs are born through WNT-driven asymmetric divisions at a stage that occurs long before establishment of the HF bulge niche. Moreover, and in striking contrast to an adult niche, SC identity in early development is acquired by the daughter that moves *away* from its parent's microenvironment. Furthermore, the paucity of WNT-signaling distributed to the SC daughter allows it to receive a paracrine SHH signal produced by its WNT^{hi} parent. This interaction leads not only to reinforced levels of the HF-SC master regulator, SOX9, but also to further suppression of *Lef1*, allowing SC progenitors to expand through symmetric and escape the WNT^{hi} slow-cycling asymmetric division status of its parent.

A final conundrum is how, in a system like this one, SC numbers become controlled. In part, the answer likely stems from the temporal distancing of uppermost, proliferating $SOX9^{+}$

SCs from their SHH-signaling center, reminiscent of what happens in the adult hair cycle (Hsu et al., 2014). More importantly, this aspect alone cannot be sufficient to control SC numbers when the niche has not yet formed, since parental WNT^{hi} *Shh*-expressing daughters would otherwise continue to churn out $SOX9^{+}$ SC daughters. Surprisingly, as morphogenesis proceeds, the daughter fate switches, so that SC production stops, and the pocket starts generating differentiating hair lineages.

Our findings provide many new and provocative insights into how SCs are specified and governed during embryogenesis, at a time preceding niche establishment. While other signaling pathways likely intersect the circuitry, antagonism between WNT and SHH pathways is crucial not only in balancing asymmetric and symmetric cell divisions, but also in delineating cellular fates and proliferation rates. Our findings illuminate why both signaling pathways have such profound impact on cancers of the skin, where spindle orientations, cellular fates, and proliferative rates are imbalanced (Beronja et al., 2013;Blanpain and Simons, 2013; Larsimont et al., 2015). Our results also pave the way for delving further into how these two signaling pathways establish their antagonistic interplay in morphogenesis and SC establishment.

EXPERIMENTAL PROCEDURES

Mice

Strains and additional details are in the Extended Experimental Procedures. K14-rtTA was activated by feeding mice with doxycycline (2 mg/kg) chow at times specified. CreER was activated to induce clonal recombination in embryos by administering a single dose of tamoxifen (4mg per dam) by oral gavage to the mother. 48h later was empirically determined to be sufficient to allow most clones labeled to consist of 1–3 cells. For LV-*PGK*-driven CreER, tamoxifen was administered at E15.5 to monitor peak placode formation. EdU (25 μg/g) was injected i.p. for 4h before lethal administration of CO_2 to the mother. Ultrasound-guided LV injection procedures have been described (Beronja et al., 2010). Animals were maintained in an AAALAC-approved animal facility, and procedures were performed with IACUC-approved protocols.

Statistical Analyses

Figures: *p<0.05; **p<0.01; ***p<0.001; ****p<0.0001; n.s. not significant. Figure 1B,F: Fisher's exact t test. Figures 2B; 4B,D: Paired t tests. Figures 5B,D; 6E: Unpaired t tests. Figure 6I: Significance test of slopes from linear regression.

Immunofluorescence Sample Preparation and Imaging

For immunofluorescence, embryos were fixed in 4% PFA in PBS for 1h at room temperature and washed in PBS. For whole-mount or tissue sections, samples were permeabilized for 3 hours in 0.3% Triton X-100 in PBS, or embedded in OCT (Tissue Tek) and cut at a thickness of 10μm. Tissue samples were then blocked in Gelatin Block or M.O.M. blocking kit (Vector). Primary antibodies were incubated at 4C overnight, secondary antibodies for 2h at room temperature and mounted in ProLong Gold (Life Tech). Epifluorescence images were acquired with an Axio Oberver.Z1 microscope equipped with an ApoTome.2 (Carl Zeiss)

slider. Confocal images were acquired with a Zeiss LSM780 laser-scanning microscope (Carl Zeiss).

Live Imaging

Fluorescently labeled E14.5 mouse embryos were placed with their dorsal side flush against the membrane of a 35-mm Lumox-bottom dish (Sarstedt). Each embryo was immobilized and further stabilized in an agarose solution comprised of 2% low-melting SeaPlaque Agarose (Cambrex) in a solution of epidermal culture medium. After equilibrating at 37°C and 5% CO_2 for ~2h, imaging was then performed on an inverted Volocity-driven spinning disk confocal system (PerkinElmer) at intervals of 8–15 min for up 18 h (491 and 561 nm laser beams, 20× air objective N.A. 0.75). During imaging, the embryo was maintained at 37°C and 5% CO_2. Overlapping regions were stitched with custom-written code in MATLAB, and resultant 4D images analyzed in ImageJ.

Supplementary Material

Refer to Web version on PubMed Central for supplementary material.

Acknowledgments

We thank the following for mice/reagents: R Kucherlapati (Harvard), R. Kemler (Max-Planck, Freiburg), H. Westphal (NIH), A. McMahon (U Southern California). We thank Fuchs Lab members: C. P. Lu, S. Beronja, N. Oshimori, R. Adam, and C. A. Rascon for helpful comments and discussions; J. Racelis for technical assistance; L. Polak, J. Levorse, and S. Hacker for assistance with mouse handling and experiments. We thank Comparative Bioscience Center (AAALAC accredited) for care of mice in accordance with National Institutes of Health (NIH) guidelines, the Flow Cytometry facility (S. Mazel, Director), the Bio-Imaging Resource Center (A. North, Director). E.F. is an Investigator of the Howard Hughes Medical Institute (HHMI). T.O. is an HHMI International Graduate Student Fellow. I.M. was the recipient of a Rockefeller University Women & Science Postdoctoral Fellowship. This material is based upon work supported by the National Science Foundation Postdoctoral Research Fellowship in Biology to A.F.M. under Award DBI-1401728. This study was supported by grants from the NIH (T32-CA009673-37 to V.F.F. and R37-AR27883 and R01-AR31737 to E.F.).

References

Adam RC, Yang H, Rockowitz S, Larsen SB, Nikolova M, Oristian DS, Polak L, Kadaja M, Asare A, Zheng D, et al. Pioneer factors govern super-enhancer dynamics in stem cell plasticity and lineage choice. Nature. 2015; 521:366–370. [PubMed: 25799994]

Ahtiainen L, Lefebvre S, Lindfors PH, Renvoise E, Shirokova V, Vartiainen MK, Thesleff I, Mikkola ML. Directional cell migration, but not proliferation, drives hair placode morphogenesis. Dev Cell. 2014; 28:588–602. [PubMed: 24636260]

Andl T, Reddy ST, Gaddapara T, Millar SE. WNT signals are required for the initiation of hair follicle development. Dev Cell. 2002; 2:643–653. [PubMed: 12015971]

Astudillo P, Larrain J. Wnt signaling and cell-matrix adhesion. Current molecular medicine. 2014; 14:209–220. [PubMed: 24467207]

Azzolin L, Panciera T, Soligo S, Enzo E, Bicciato S, Dupont S, Bresolin S, Frasson C, Basso G, Guzzardo V, et al. YAP/TAZ incorporation in the beta-catenin destruction complex orchestrates the Wnt response. Cell. 2014; 158:157–170. [PubMed: 24976009]

Baeg GH, Lin X, Khare N, Baumgartner S, Perrimon N. Heparan sulfate proteoglycans are critical for the organization of the extracellular distribution of Wingless. Development. 2001; 128:87–94. [PubMed: 11092814]

Beronja S, Janki P, Heller E, Lien WH, Keyes BE, Oshimori N, Fuchs E. RNAi screens in mice identify physiological regulators of oncogenic growth. Nature. 2013; 501:185–190. [PubMed: 23945586]

Beronja S, Livshits G, Williams S, Fuchs E. Rapid functional dissection of genetic fetworks via tissue specific transduction and RNAi in mouse embryos. Nature Medicine. 2010; 16:821–827.

Bhat KM, Schedl P. Establishment of stem cell identity in the Drosophila germline. Dev Dyn. 1997; 210:371–382. [PubMed: 9415423]

Blanpain C, Fuchs E. Stem cell plasticity. Plasticity of epithelial stem cells in tissue regeneration. Science. 2014; 344:1242281. [PubMed: 24926024]

Blanpain C, Simons BD. Unravelling stem cell dynamics by lineage tracing. Nat Rev Mol Cell Biol. 2013; 14:489–502. [PubMed: 23860235]

Brizzi MF, Tarone G, Defilippi P. Extracellular matrix, integrins, and growth factors as tailors of the stem cell niche. Curr Opin Cell Biol. 2012; 24:645–651. [PubMed: 22898530]

Cabello J, Neukomm LJ, Gunesdogan U, Burkart K, Charette SJ, Lochnit G, Hengartner MO, Schnabel R. The Wnt pathway controls cell death engulfment, spindle orientation, and migration through CED-10/Rac. PLoS Biol. 2010; 8:e1000297. [PubMed: 20126385]

Clayton E, Doupe DP, Klein AM, Winton DJ, Simons BD, Jones PH. A single type of progenitor cell maintains normal epidermis. Nature. 2007; 446:185–189. [PubMed: 17330052]

Clevers H, Loh KM, Nusse R. Stem cell signaling. An integral program for tissue renewal and regeneration: Wnt signaling and stem cell control. Science. 2014; 346:1248012. [PubMed: 25278615]

Dansereau DA, Lasko P. The development of germline stem cells in Drosophila. Methods Mol Biol. 2008; 450:3–26. [PubMed: 18370048]

DasGupta R, Fuchs E. Multiple roles for activated LEF/TCF transcription complexes during hair follicle development and differentiation. Development. 1999; 126:4557–4568. [PubMed: 10498690]

Etienne-Manneville S, Hall A. Cdc42 regulates GSK-3beta and adenomatous polyposis coli to control cell polarity. Nature. 2003; 421:753–756. [PubMed: 12610628]

Gao C, Chen G, Kuan SF, Zhang DH, Schlaepfer DD, Hu J. FAK/PYK2 promotes the Wnt/beta-catenin pathway and intestinal tumorigenesis by phosphorylating GSK3beta. eLife. 2015; 4

Gat U, DasGupta R, Degenstein L, Fuchs E. De Novo hair follicle morphogenesis and hair tumors in mice expressing a truncated beta-catenin in skin. Cell. 1998; 95:605–614. [PubMed: 9845363]

Greco V, Chen T, Rendl M, Schober M, Pasolli HA, Stokes N, Dela Cruz-Racelis J, Fuchs E. A two-step mechanism for stem cell activation during hair regeneration. Cell Stem Cell. 2009; 4:155–169. [PubMed: 19200804]

Habib SJ, Chen BC, Tsai FC, Anastassiadis K, Meyer T, Betzig E, Nusse R. A localized Wnt signal orients asymmetric stem cell division in vitro. Science. 2013; 339:1445–1448. [PubMed: 23520113]

Hsu YC, Li L, Fuchs E. Transit-amplifying cells orchestrate stem cell activity and tissue regeneration. Cell. 2014; 157:935–949. [PubMed: 24813615]

Hsu YC, Pasolli HA, Fuchs E. Dynamics between stem cells, niche, and progeny in the hair follicle. Cell. 2011; 144:92–105. [PubMed: 21215372]

Huelsken J, Vogel R, Erdmann B, Cotsarelis G, Birchmeier W. beta-Catenin controls hair follicle morphogenesis and stem cell differentiation in the skin. Cell. 2001; 105:533–545. [PubMed: 11371349]

Jamora C, DasGupta R, Kocieniewski P, Fuchs E. Links between signal transduction, transcription and adhesion in epithelial bud development. Nature. 2003; 422:317–322. [PubMed: 12646922]

Karlsson L, Bondjers C, Betsholtz C. Roles for PDGF-A and sonic hedgehog in development of mesenchymal components of the hair follicle. Development. 1999; 126:2611–2621. [PubMed: 10331973]

Kodama A, Karakesisoglou I, Wong E, Vaezi A, Fuchs E. ACF7: an essential integrator of microtubule dynamics. Cell. 2003; 115:343–354. [PubMed: 14636561]

Kuraguchi M, Wang XP, Bronson RT, Rothenberg R, Ohene-Baah NY, Lund JJ, Kucherlapati M, Maas RL, Kucherlapati R. Adenomatous polyposis coli (APC) is required for normal development of skin and thymus. PLoS Genet. 2006; 2:e146. [PubMed: 17002498]

Larsimont JC, Youssef KK, Sanchez-Danes A, Sukumaran V, Defrance M, Delatte B, Liagre M, Baatsen P, Marine JC, Lippens S, et al. Sox9 Controls Self-Renewal of Oncogene Targeted Cells and Links Tumor Initiation and Invasion. Cell Stem Cell. 2015; 17:60–73. [PubMed: 26095047]

Lechler T, Fuchs E. Asymmetric cell divisions promote stratification and differentiation of mammalian skin. Nature. 2005; 437:275–280. [PubMed: 16094321]

Li VS, Ng SS, Boersema PJ, Low TY, Karthaus WR, Gerlach JP, Mohammed S, Heck AJ, Maurice MM, Mahmoudi T, et al. Wnt signaling through inhibition of beta-catenin degradation in an intact Axin1 complex. Cell. 2012; 149:1245–1256. [PubMed: 22682247]

Lustig B, Jerchow B, Sachs M, Weiler S, Pietsch T, Karsten U, van de Wetering M, Clevers H, Schlag PM, Birchmeier W, et al. Negative feedback loop of Wnt signaling through upregulation of conductin/axin2 in colorectal and liver tumors. Mol Cell Biol. 2002; 22:1184–1193. [PubMed: 11809809]

Mendoza-Topaz C, Mieszczanek J, Bienz M. The Adenomatous polyposis coli tumour suppressor is essential for Axin complex assembly and function and opposes Axin's interaction with Dishevelled. Open Biol. 2011; 1:110013. [PubMed: 22645652]

Noramly S, Freeman A, Morgan BA. beta-catenin signaling can initiate feather bud development. Development. 1999; 126:3509–3521. [PubMed: 10409498]

Nowak JA, Polak L, Pasolli HA, Fuchs E. Hair follicle stem cells are specified and function in early skin morphogenesis. Cell Stem Cell. 2008; 3:33–43. [PubMed: 18593557]

Pardo-Saganta A, Tata PR, Law BM, Saez B, Chow R, Prabhu M, Gridley T, Rajagopal J. Parent stem cells can serve as niches for their daughter cells. Nature. 2015; 523:597–601. [PubMed: 26147083]

Pei Y, Brun SN, Markant SL, Lento W, Gibson P, Taketo MM, Giovannini M, Gilbertson RJ, Wechsler-Reya RJ. WNT signaling increases proliferation and impairs differentiation of stem cells in the developing cerebellum. Development. 2012; 139:1724–1733. [PubMed: 22461560]

Reya T, Duncan AW, Ailles L, Domen J, Scherer DC, Willert K, Hintz L, Nusse R, Weissman IL. A role for Wnt signalling in self-renewal of haematopoietic stem cells. Nature. 2003; 423:409–414. [PubMed: 12717450]

Rhee H, Polak L, Fuchs E. Lhx2 maintains stem cells character in hair follicles. Science. 2006; 312:1946–1949. [PubMed: 16809539]

Sakaue-Sawano A, Kurokawa H, Morimura T, Hanyu A, Hama H, Osawa H, Kashiwagi S, Fukami K, Miyata T, Miyoshi H. Visualizing Spatiotemporal Dynamics of Multicellular Cell-Cycle Progression. Cell. 2008; 132:487–498. [PubMed: 18267078]

Scadden DT. Nice neighborhood: emerging concepts of the stem cell niche. Cell. 2014; 157:41–50. [PubMed: 24679525]

Schofield R. The relationship between the spleen colony-forming cell and the haemopoietic stem cell. Blood cells. 1978; 4:7–25. [PubMed: 747780]

Shin K, Lee J, Guo N, Kim J, Lim A, Qu L, Mysorekar IU, Beachy PA. Hedgehog/Wnt feedback supports regenerative proliferation of epithelial stem cells in bladder. Nature. 2011; 472:110–114. [PubMed: 21389986]

Shyer AE, Huycke TR, Lee C, Mahadevan L, Tabin CJ. Bending gradients: how the intestinal stem cell gets its home. Cell. 2015; 161:569–580. [PubMed: 25865482]

Song X, Zhu CH, Doan C, Xie T. Germline stem cells anchored by adherens junctions in the Drosophila ovary niches. Science. 2002; 296:1855–1857. [PubMed: 12052957]

St-Jacques B, Dassule HR, Karavanova I, Botchkarev VA, Li J, Danielian PS, McMahon JA, Lewis PM, Paus R, McMahon AP. Sonic hedgehog signaling is essential for hair development. Curr Biol. 1998; 8:1058–1068. [PubMed: 9768360]

Sugimura R, He XC, Venkatraman A, Arai F, Box A, Semerad C, Haug JS, Peng L, Zhong XB, Suda T, et al. Noncanonical Wnt signaling maintains hematopoietic stem cells in the niche. Cell. 2012; 150:351–365. [PubMed: 22817897]

Sugioka K, Mizumoto K, Sawa H. Wnt regulates spindle asymmetry to generate asymmetric nuclear beta-catenin in C. elegans. Cell. 2011; 146:942–954. [PubMed: 21925317]

van Genderen C, Okamura RM, Farinas I, Quo RG, Parslow TG, Bruhn L, Grosschedl R. Development of several organs that require inductive epithelial-mesenchymal interactions is impaired in LEF-1-deficient mice. Genes Dev. 1994; 8:2691–2703. [PubMed: 7958926]

Vidal VP, Chaboissier MC, Lutzkendorf S, Cotsarelis G, Mill P, Hui CC, Ortonne N, Ortonne JP, Schedl A. Sox9 is essential for outer root sheath differentiation and the formation of the hair stem cell compartment. Curr Biol. 2005; 15:1340–1351. [PubMed: 16085486]

Williams SE, Beronja S, Pasolli HA, Fuchs E. Asymmetric cell divisions promote Notch-dependent epidermal differentiation. Nature. 2011; 470:353–358. [PubMed: 21331036]

Williams SE, Ratliff LA, Postiglione MP, Knoblich JA, Fuchs E. Par3-mInsc and Galphai3 cooperate to promote oriented epidermal cell divisions through LGN. Nat Cell Biol. 2014; 16:758–769. [PubMed: 25016959]

Woo WM, Zhen HH, Oro AE. Shh maintains dermal papilla identity and hair morphogenesis via a Noggin-Shh regulatory loop. Genes Dev. 2012; 26:1235–1246. [PubMed: 22661232]

Yamashita YM, Jones DL, Fuller MT. Orientation of asymmetric stem cell division by the APC tumor suppressor and centrosome. Science. 2003; 301:1547–1550. [PubMed: 12970569]

Zhu CH, Xie T. Clonal expansion of ovarian germline stem cells during niche formation in Drosophila. Development. 2003; 130:2579–2588. [PubMed: 12736203]

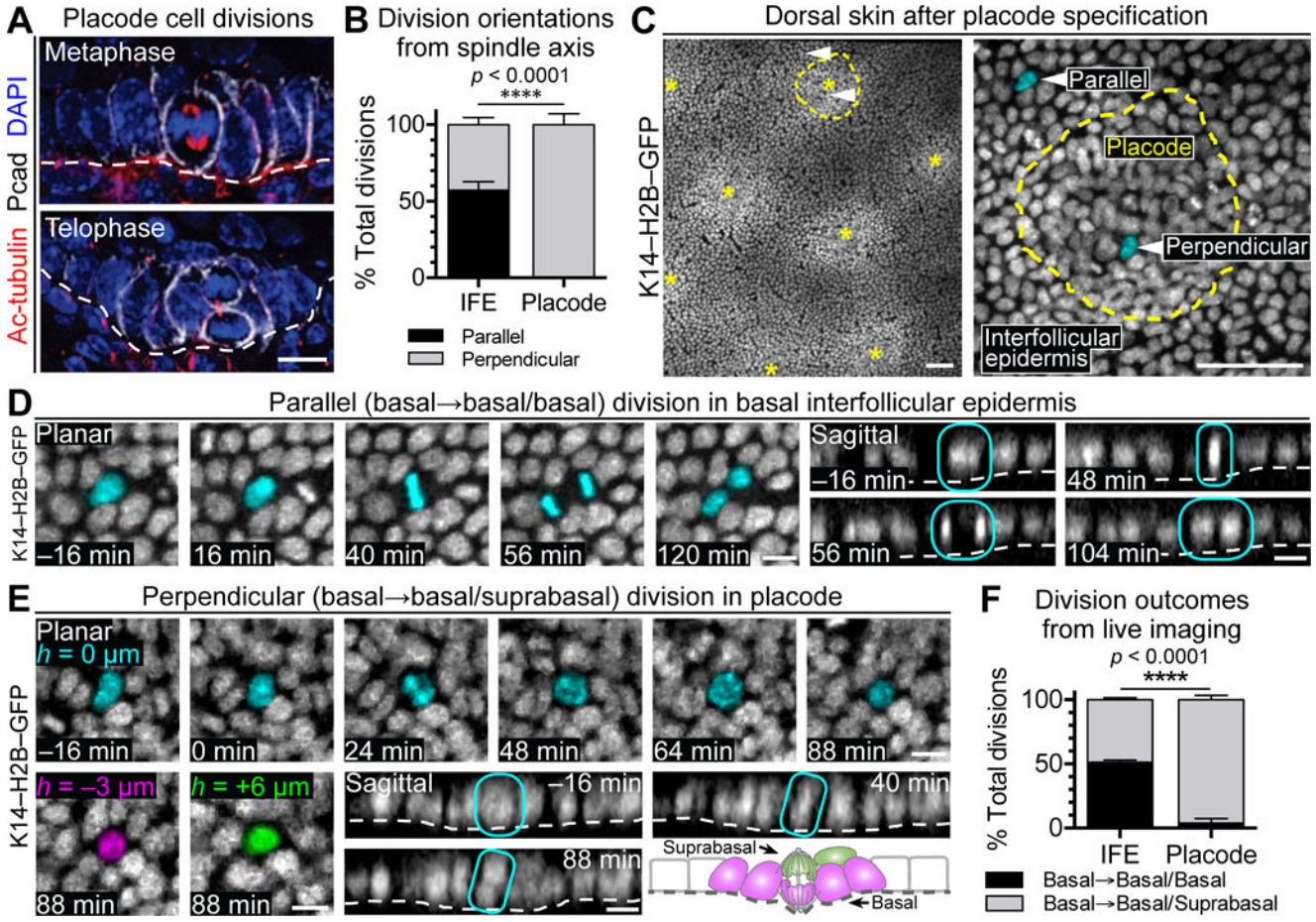

Figure 1. Cells Divide Perpendicularly in Hair Placodes

(A) Perpendicular divisions during metaphase (top) and telophase (bottom) in mouse hair placodes.

(B) Quantification of parallel and perpendicular division orientation based on spindle axis of basal cells in interfollicular epidermis (IFE) and placodes. Data are % ± standard deviation (SD) from pooled counts in n=3 embryos, 41 placodes, 187 IFE divisions.

(C) E14.5 dorsal skin visualized by live imaging of K14–H2B–GFP embryos. (Left) Stitched image of placodes (asterisks) and IFE. (Right) Placode (yellow outline) surrounded by IFE. Arrows indicate examples of a parallel or perpendicular division, depicted in (D,E), respectively. See Movie S1.

(D) Time course from live imaging of parallel division in basal IFE. (Left) Planar views centered in basal plane with dividing cell pseudo-colored cyan. (Right) Sagittal views reconstructed from confocal stacks. Dividing cell circled in cyan. See Movie S2.

(E) Time course from live imaging of perpendicular division in placode. (Top) Planar views centered in basal plane at height 0µm, with dividing cell pseudo-colored cyan. (Bottom left) Planar views after mitosis indicating pseudo-colored basal daughter at −3µm (left, magenta) and suprabasal daughter at +6µm (right, green). (Bottom right) Sagittal views reconstructed from confocal stacks. Dividing cell circled in cyan. Schematic of perpendicular placode division. See Movie S3.

(F) Quantifications of division outcomes in IFE and placodes based on live imaging of placodes. Data are mean % ± SD from 322 divisions, n=3 embryos.
In (D,E), t=0 corresponds to onset of mitosis as determined by DNA condensation.
Tissues processed as indicated for immunofluorescence microscopy (IMF) (Acetylated-tubulin, Pcad) or endogenous fluorescence (H2B–GFP).
White dashed lines indicate basement membrane.
All scales bars, 10μm, except (C), 50μm.

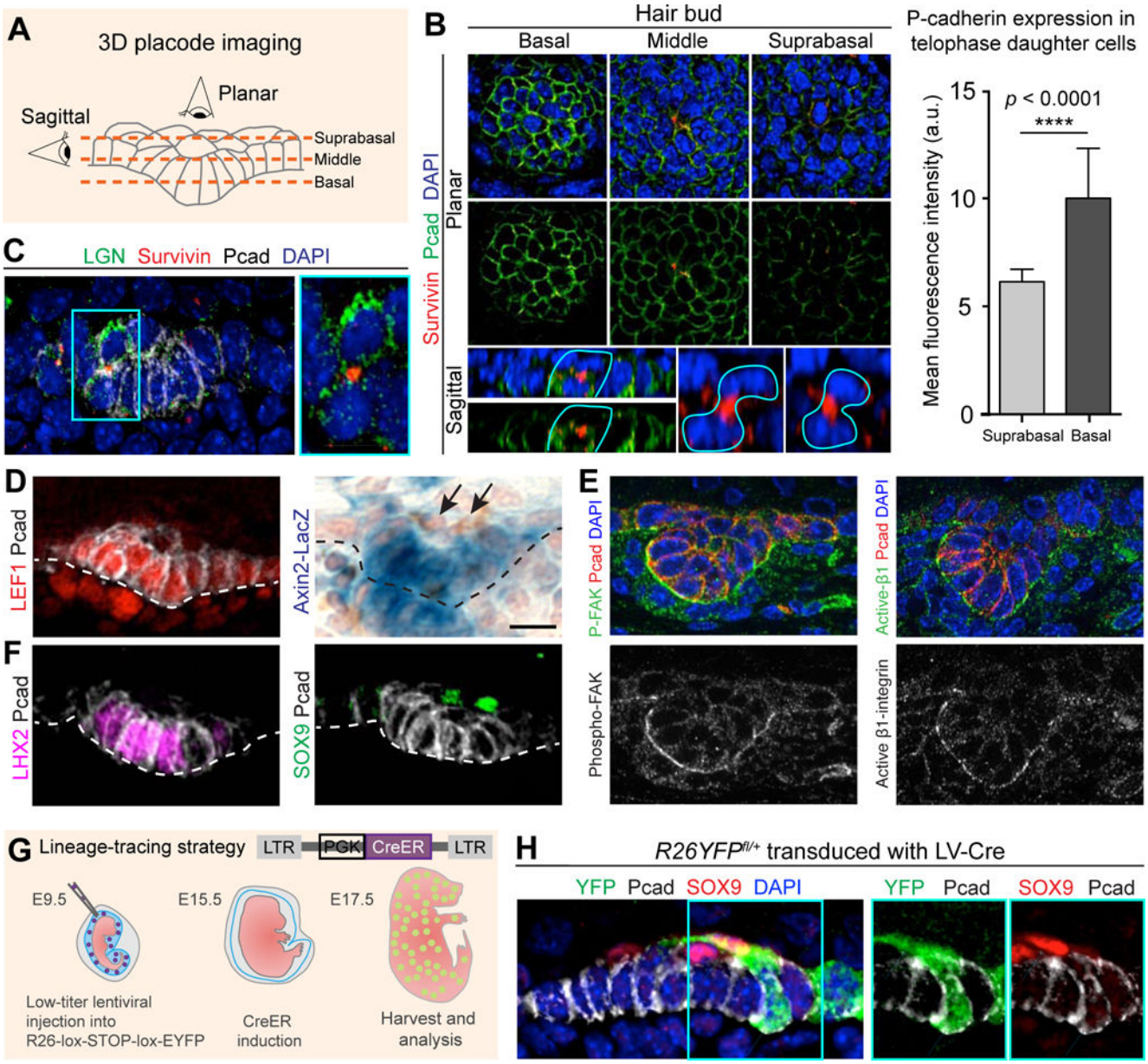

Figure 2. Asymmetric Divisions in Hair Buds Generate WNT^{hi} Basal and WNT^{lo} Suprabasal Cells

(A) Schematic of epithelial bud imaging. Dashed lines mark imaging planes.

(B) (Left) Planar and sagittal projections through hair placode, subjected to whole-mount IMF. Pcad enriched in basal cells. Vertical division (asterisk) marked by Survivin (arrows) to identify midbody of late-stage mitotic daughters (cyan lines). (Right) Quantifications of Pcad IMF. Data (mean ± SD) are from 3 embryos (n=26 doublets).

(C) Suprabasal enrichment of LGN (arrow) in hair placode.

(D) IMF or X-gal staining of WT placodes. Note absence of WNT-signaling in suprabasal cells (arrows).

(E) Basal enrichment (arrows) of phospho-Tyr397 (P)-Focal Adhesion Kinase (FAK) and active β1-integrin in hair buds.

(F) IMF of WT placodes. Note $SOX9^{+}$ suprabasal placode cells (arrows).
(G) Lentiviral strategy to sparsely mark and track placode cells. LV-$CreER^{T2}$ was activated by tamoxifen gavage at E15.5 for 48h.
(H) Lineage-traced clones in placodes. Arrows mark $Pcad^{hi}$ $SOX9^{-}$ basal and $SOX9^{+}$ suprabasal cells within YFP^{+} clone.
White dashed lines indicate basement membrane.
Tissues processed as indicated for IMF (LGN, Survivin, Pcad, LEF1, P-FAK, Active β1-integrin, YFP) or X-gal (Axin2-LacZ).
All scale bars, 10μm, except lower-right sagittal views in (B), 5μm.
See also Figure S1.

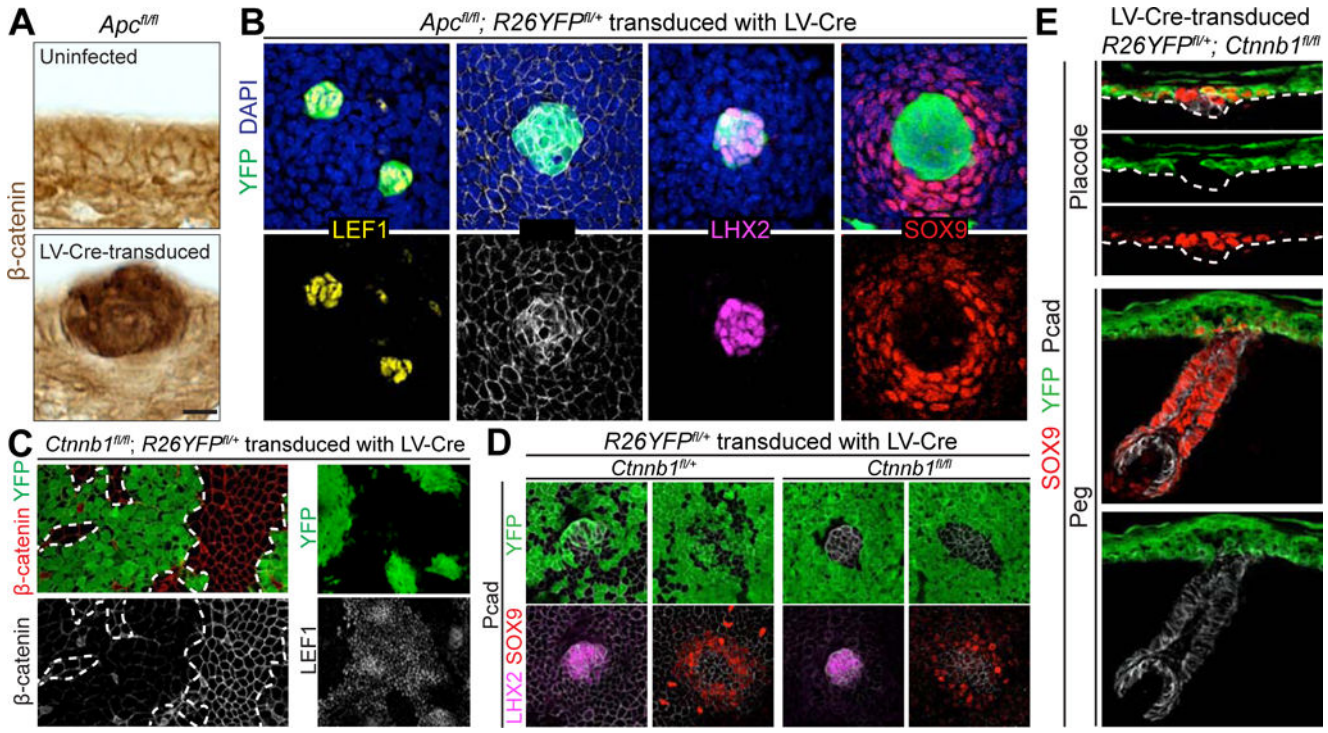

Figure 3. Juxtaposition of WNT^{hi} and WNT^{lo} Borders Is Sufficient to Acquire Asymmetric Cell Fates

(A) Immunohistochemistry of *Apc*$^{fl/fl}$ epidermis uninfected (top) or LV-Cre-transduced (bottom), generating *Apc*-null regions with increased WNT activity, indicated by intense β-catenin signal.

(B) Planar confocal IMF of *Apc*$^{fl/fl}$*; R26YFP*$^{fl/+}$ epidermis mosaic for LV-Cre. Note WNT-hyperactivated next to WNT-normal regions establish boundary for asymmetric cell fates.

(C) Planar confocal IMF in *Ctnnb1*$^{fl/fl}$*; R26YFP*$^{fl/+}$ embryos transduced with LV-Cre. Note selective loss of LEF1 in IFE patches where β-catenin is absent.

(D) Planar confocal IMF in *Ctnnb1*$^{fl/fl}$ (or $^{fl/+}$); *R26YFP*$^{fl/+}$ embryos infected with high-titer LV-Cre to generate small regions of β-catenin^{+} untransduced cells surrounded by β-catenin^{-} transduced cells.

(E) Sagittal IMF in placode (top) and peg (bottom) of *R26YFP*$^{fl/+}$*; Ctnnb1*$^{fl/fl}$ embryos transduced with LV-Cre. Bracket indicates SOX9^{+} IFE halo. Note YFP^{+} SOX9^{+} IFE cells do not contribute to mature HF.

Tissues processed as indicated for immunohistochemistry (β-catenin) or IMF (LEF1, Pcad, LHX2, SOX9, β-catenin, YFP).

Dashed lines in (A,E) indicate basement membrane, in (C), borders between transduced and untransduced regions.

Scale bars in (A), 10μm; in (B,D,E), 20μm; in (C), 50μm.

See also Figure S2.

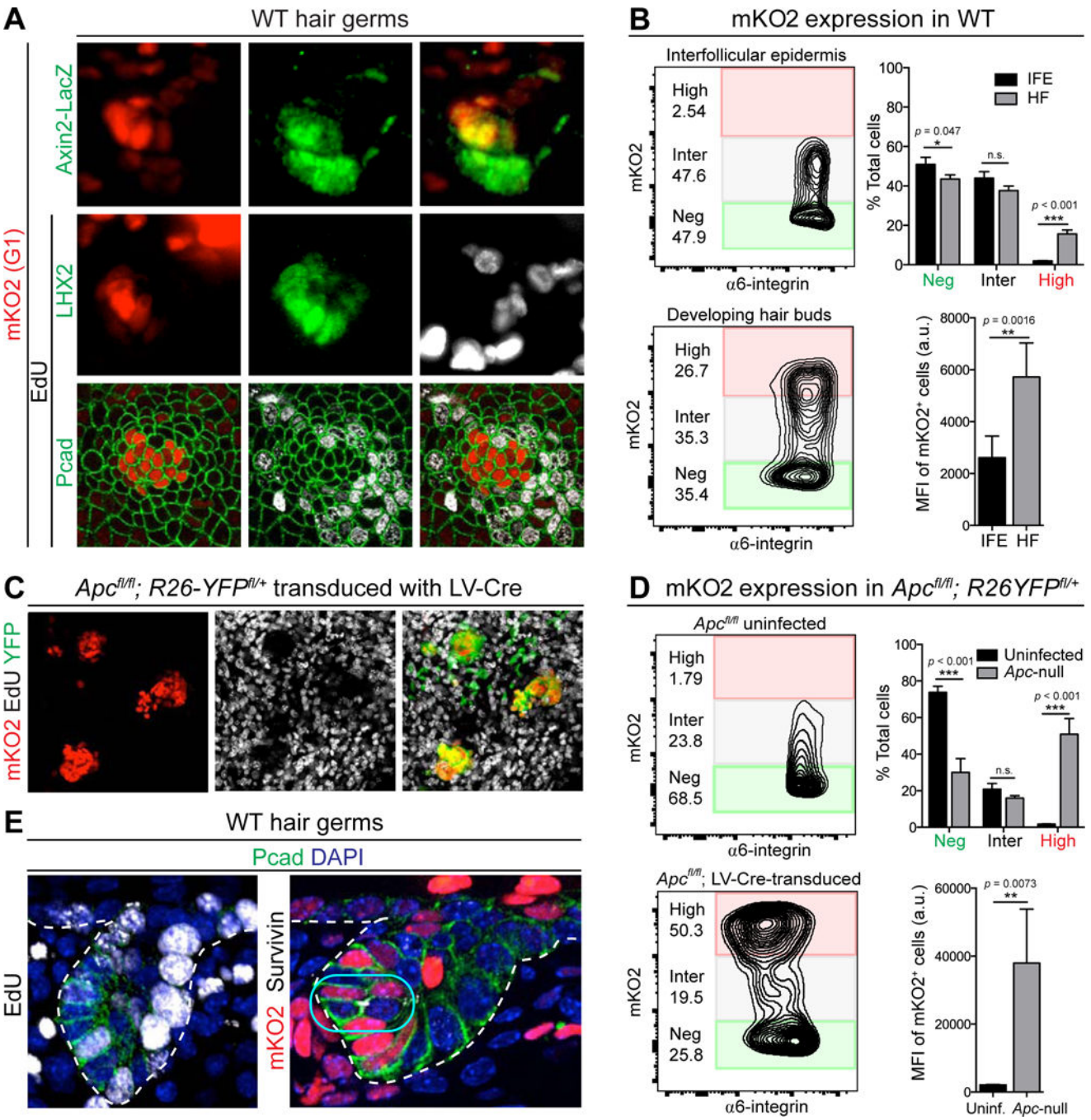

Figure 4. WNT^{hi} Hair Bud Cells are in Prolonged G_1

(A) mKO2 and IMF of skin from *Fucci; Axin2LacZ* embryo following 4h EdU. Asterisks denote terminally differentiating IFE cells.

(B) (Left) Flow-cytometry plots for α6-integrin and mKO2 in E17.5 LHX2-GFP embryonic HF (GFP$^+$) and IFE (GFP$^-$). Note significant fraction of α6^{hi} HF, but not IFE cells, are mKO2^{hi} (red box). (Right) Mean fluorescence intensities (MFI) in IFE and HF for mKO2$^+$ cells (Inter+High). Data from n=5 litters and are mean ± SD.

(C) Planar confocal IMF of epidermis from *Fucci; Apc$^{fl/fl}$; R26YFP$^{fl/+}$* embryo transduced mosaically with LV-Cre and following 4h EdU pulse. Note mKO2^{hi} and EdU^{lo} signals in WNT-hyperactive (YFP^{+}) regions.

(D) Analogous flow-cytometry plots and MFI to (B) for uninfected and LV-Cre-transduced regions of E14.5 *Apc$^{fl/fl}$* epidermis.

(E) IMF of sagittal sections of hair germs showing examples of EdU^{+} cell (left, arrow) and dividing cell (right, box) within Pcad^{hi} (WNT^{hi}) mKO2^{+} pocket.

Tissues processed as indicated for IMF (Pcad, LHX2, Axin2-LacZ, Survivin, YFP), EdU, or endogenous fluorescence (mKO2).

White dashed lines indicate basement membrane.

Scale bars in (A), 10μm; in (C), 50μm.

See also Figure S3.

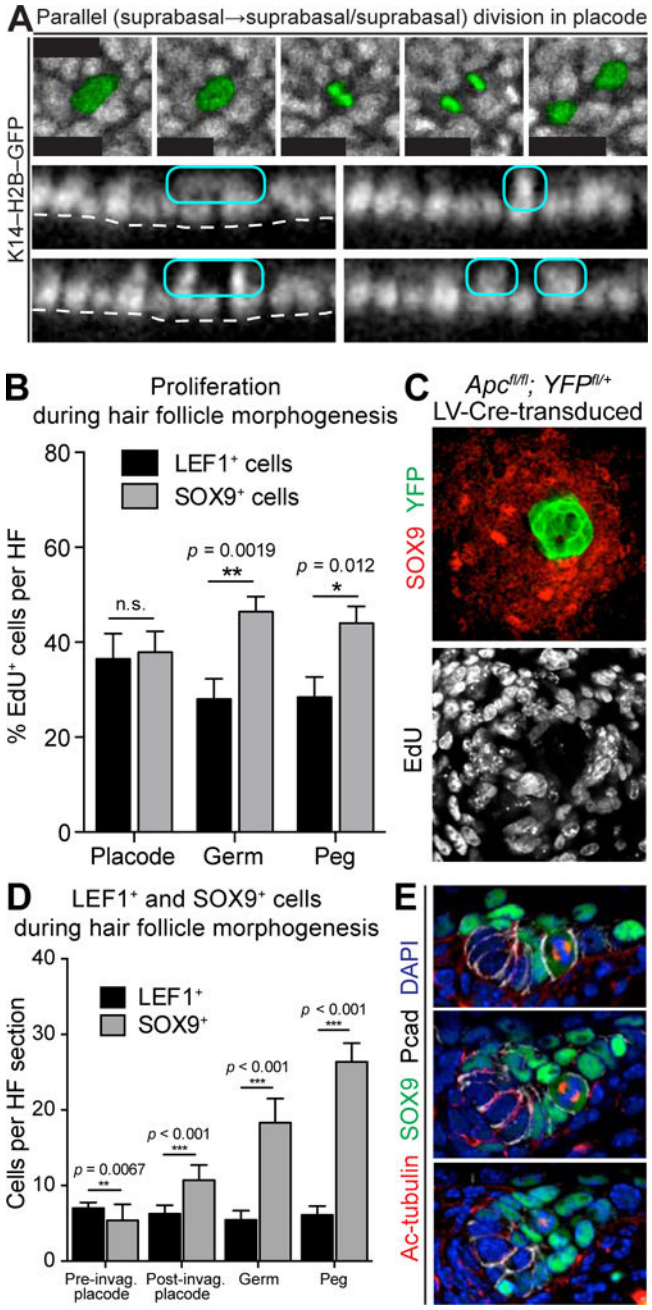

Figure 5. SOX9$^+$ Cells Expand Symmetrically During HF Morphogenesis

(A) Time course from live imaging of parallel suprabasal division in placode. (Top) Planar views centered in suprabasal plane with dividing cell pseudo-colored green. (Bottom) Sagittal views reconstructed from confocal stacks. Dividing cell circled in cyan. t=0 corresponds to onset of mitosis as determined by DNA condensation. 75 suprabasal divisions imaged from n=3 embryos. See Movie S4.

(B) Quantification of proliferation (4h EdU pulse) of SOX9$^+$ and LEF1$^+$ cells at different HF morphogenesis stages. Data from n=3 litters, 74 HFs and are mean ± SD.

(C) Planar confocal IMF of *Apc*$^{fl/fl}$; *R26YFP*$^{fl/+}$ epidermis transduced mosaically with *LV-Cre*, following 4h EdU pulse.
(D) Quantification of numbers of LEF1^{+} and SOX9^{+} cells at different HF morphogenesis stages. Data from n=3 litters, 117 HFs and are mean ± SEM.
(E) IMF of sagittal sections of HFs showing examples (arrows) of parallel, perpendicular, and suprabasal divisions in SOX9^{+} cells.
Tissues processed as indicated for IMF (SOX9, Acetylated-tubulin, Pcad, YFP) and EdU. White dashed lines indicate basement membrane.
Scale bars in (A,E), 10μm; in (C), 20μm.
See also Figure S4.

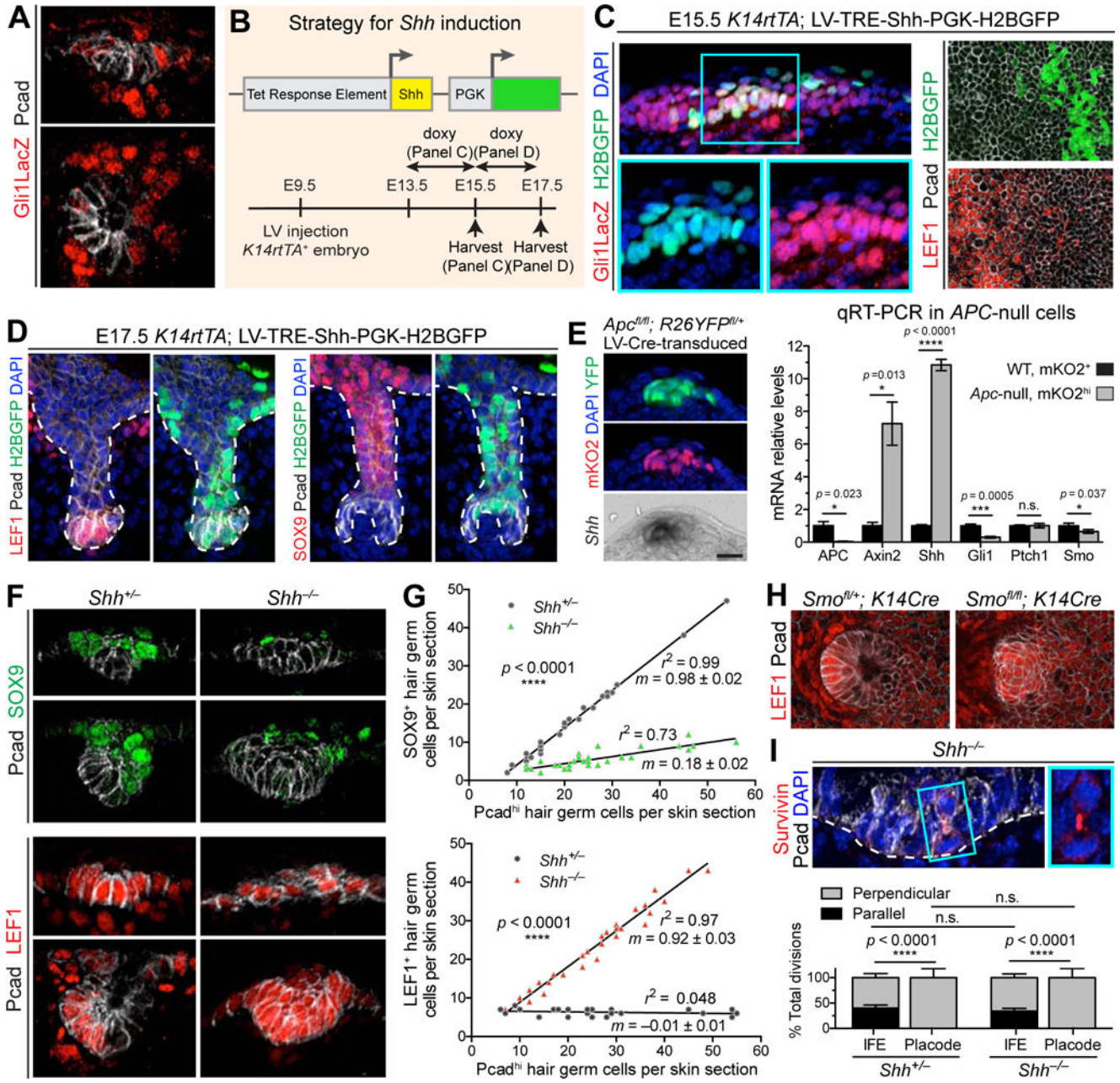

Figure 6. Antagonism Between WNT and SHH Signaling Orchestrates Differential Expansion of Two Daughter Populations

(A) IMF of sagittal sections of placode (top) and hair germ (bottom). Note low SHH-signaling (Gli1LacZ/βgal) in Pcad^{hi} cells.

(B) Strategy for activating ectopic *Shh* in embryonic epidermis.

(C) Confocal IMF of sagittal sections (Left) and planar views (Right) of E15.5 Gli1LacZ epidermis transduced with LV-TRE-Shh, induced at E13.5, and immunolabeled for Gli1-LacZ (Left) or LEF1 (Right). Boxed area is magnified. Arrows denote autocrine SHH-signaling.

(D) IMF of sagittal sections of E17.5 HFs transduced with LV-TRE-Shh, induced at E15.5. Note that once HFs start to mature, SHH-transduced pocket cells (arrows) do not show signs of LEF1 reduction or SOX9 induction.

(E) (Left) *Apc*-null cells from *Fucci; Apc*$^{fl/fl}$*; R26YFP*$^{fl/+}$ epidermis transduced with LV-Cre. Note *Shh* induced in ectopic WNT^{hi} cells. (Right) Quantitative real-time (qRT-)PCR in FACS-purified *Apc*-null and WT cells from n=3 litters, mean ± SD.

(F) IMF of sagittal sections of *Shh*$^{-/-}$ and *Shh*$^{+/-}$ hair placode and germ.

(G) Quantifications of SOX9^{+} and LEF1^{+} cells relative to number of Pcad^{+} cells in sagittal sections of *Shh*$^{-/-}$ and *Shh*$^{+/-}$ HFs. *m* is slope ± standard error. r^2 is coefficient of determination. Epithelial buds of same stage and size were compared from n=3 embryos, 54 HFs for SOX9, 105 HFs for LEF1.

(H) Planar confocal IMF of epithelial-specific *Smoothened* heterozygote and *Smoothened*-null hair bud showing LEF1 expanded suprabasally (brackets), as in *Shh*-null embryo.

(I) (Top) IMF of sagittal sections of *Shh*$^{-/-}$ hair bud showing perpendicular divisions occurring independently of SHH-signaling (boxed region magnified at right). (Bottom) Quantifications of division orientations in IFE and placodes of *Shh*$^{+/-}$ and *Shh*$^{-/-}$ placodes. Measurements based on spindle axis visualized by survivin and DAPI. Data are % ± SD (*Shh*$^{-/-}$: 30 divisions in 13 HFs, 116 divisions in IFE; *Shh*$^{+/-}$: 31 divisions in 11 HFs; 98 divisions in IFE).

Tissues processed as indicated for IMF (Gli1LacZ/βgal, Pcad, LEF1, SOX9, Survivin, YFP) or epifluorescence (mKO2).

White dashed lines indicate basement membrane.

All scale bars, 10μm, except in (C,H), 20μm.

See also Figure S5.

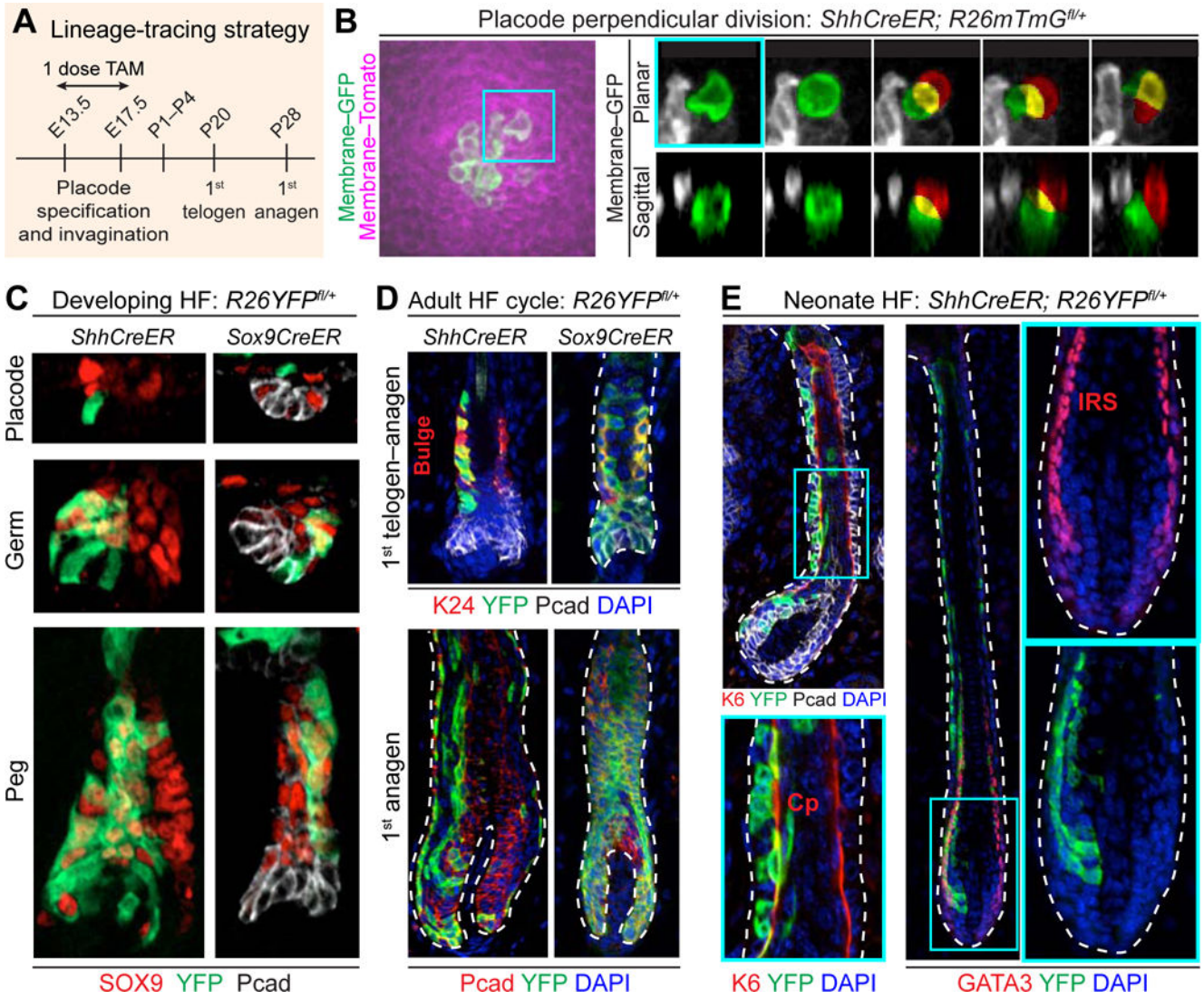

Figure 7. SHH^{+} Cells Generate SOX9^{+} Stem Cells Early but Differentiation Lineages Late in HF Morphogenesis

(A) Strategy to lineage-trace embryonic SHH^{+} and SOX9^{+} cells. *ShhCreER; R26mTmG$^{fl/+}$*, *ShhCreER; R26YFP$^{fl/+}$*, and *Sox9CreER; R26YFP$^{fl/+}$* embryos were treated with tamoxifen (TAM) once during window of HF morphogenesis and harvested at indicated times.

(B) Live imaging of perpendicular division of SHH^{+} placode cell. (Left) Labeled membrane shows SHH^{+} (GFP^{+}) cells within a placode. (Right) Time course of maximum-intensity projections of planar confocal stacks (Top) and sagittal reconstructions (Bottom) of perpendicular division of SHH^{+} placode cell (green) leading to a basal (green) and suprabasal (red) cell (overlap, yellow). t=0 corresponds to onset of mitosis as determined by cell rounding. See Movie S5.

(C) Examples of lineage tracings of SHH^{+} cells marked at early stages of HF morphogenesis. Note that SHH^{+} cells give rise to SOX9^{+} cells, but SOX9^{+} cells do not generate Pcad^{hi} SHH^{+} cells.

(D) Examples of lineage tracings monitored to 1st telogen and anagen. Note *ShhCreER; R26YFP*$^{+}$ (and *Sox9CreER*) labeled cells contribute to adult SC pool (K24+) (bracket), and to all HF lineages in subsequent hair cycle (bottom).

(E) Examples of lineage tracings from cells marked at later stages of HF morphogenesis and monitored to HF maturation (P1–4). Note that SHH^{+} cells marked at later times give rise to differentiated lineages: K6, companion layer (Cp, arrows); GATA3, inner root sheath (IRS, arrows).

Tissues processed as indicated for IMF (SOX9, YFP, Pcad, K24, K6, GATA3) or endogenous fluorescence (GFP, Tomato).

White dashed lines indicate basement membrane.

All scale bars, 10μm.